Application note

# Distribution of Defects & Impurities in Diamonds Probed by Infrared and Photoluminescence Imaging

Diamond is a multifunctional material known for its exceptional optical, electronic, thermal, mechanical, and chemical properties. Diamond is an allotrope of carbon, with tetrahedra of carbon atoms forming a cubic structure. Impurities and defects are common in natural diamonds but less prevalent in synthetic diamonds. The presence of impurities can alter the properties of diamond such as imparting color. Diamonds are classified based on the presence and quantity of impurities and defects. From a geological view point, the flaws (impurities and defects) provide clues to the formation and thermal history of the diamond.

Nitrogen is the most common impurity in diamonds that substitutes for carbon atoms in the lattice. Diamonds that contain detectible levels of nitrogen impurities are classified as type I diamonds whereas type II diamonds contain no detectable nitrogen. The arrangement of nitrogen in the diamond lattice is used to further classify diamonds. Diamonds with isolated nitrogen substitutions (C-centers) are classified as Type Ib whereas those containing aggregated nitrogen are classified as Type Ia. If pairs of nitrogen atoms ($N_2$) are formed, they are known as A-centers (IaA) and if 4 nitrogen atoms are clustered around a vacancy ($N_4V$) in the structure, they are called B-centers (IaB). A full discussion of the complexity of type classifying diamonds is beyond the scope of this application note.

Infrared spectroscopy is well established as a primary technique used in assessing the nitrogen content and the aggregation of nitrogen in diamonds as well as other structural features. Photoluminescence (PL) is another commonly used spectroscopic technique for detecting different forms of nitrogen impurities in diamonds. PL is a process in which a molecule absorbs a photon in the visible region, exciting one of its electrons to a higher electronic excited state, and then radiates a photon as the electron returns to a lower energy state. With PL the emitted light occurs at a longer wavelength than the incident light, and with Raman spectroscopy the scattered Raman light is also typically measured at longer wavelengths (Stokes scatter) than the incident (laser) light. This has the consequence that the incident laser light used in Raman spectroscopy can produce both photoluminescence peaks and Raman peaks comingled in the same spectrum.

FTIR, Raman, and PL spectroscopy are complementary techniques for diamond analysis, each providing unique insights into the material's properties. FTIR spectroscopy excels in detecting impurities and defect structures and is the technique of choice for type classification, which is essential for gemological analysis and many industrial applications. Raman spectroscopy provides information about diamonds' lattice vibrations and structural integrity, as well as strain and stress. Raman spectroscopy can also identify inclusions within diamonds. PL spectroscopy reveals electronic states and luminescence properties. By analyzing the PL emission lines, specific defect centers and their charge states can be identified. Together, these techniques offer a holistic approach to understanding and characterizing diamonds in gemology and materials science.

## Experimental

The sample analyzed was a small natural diamond, approximately dimensions of 3.5 mm x 2.8 mm and ~0.5 mm. The infrared mapping was performed using a Thermo Scientific™ Nicolet™ RaptIR+™ FTIR microscope using the 15X infrared objective. The sample area analyzed was a 1000 µm x 1000 µm region using a 25 µm x 25 µm aperture and 25 µm steps. FTIR data was collected in transmission mode through the sample. The PL data was collected as part of the Raman imaging experiment using a Thermo Scientific™ DXR3xi Raman Imaging microscope configured with a 532 nm laser and a 50X objective. Raman spectra were collected every 10 µm over the same area used in the infrared mapping (1000 µm x 1000 µm). To get 3-D data, the same area was imaged at 40 different focal positions using 5-µm steps (200 µm total) down into the sample.

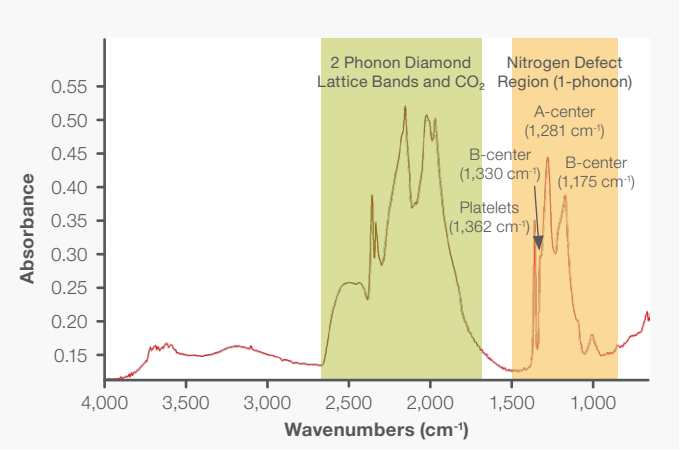


**Figure 1. A representative infrared spectrum from the diamond sample. The 2-phonon diamond lattice bands are shown in the green highlighted region and the yellow highlighted region contains the nitrogen defect peaks.**

## Results

Figure 1 shows a representative infrared spectrum from the diamond sample where the regions for nitrogen defects (1-phonon region) and the 2-phonon diamond lattice bands are highlighted. Clearly, this diamond sample contains a significant amount of nitrogen impurities. The peak at 1,281 $cm^{-1}$ is attributed to the A centers ($N_2$); the 1,330 $cm^{-1}$ and 1,175 $cm^{-1}$ peaks are assigned to the B centers ($N_4V$); and the sharp peak at 1,362 $cm^{-1}$ indicates the presence of the platelets (B' defects). Platelets are not directly nitrogen substitution defects but thin, planar layers of carbon interstitials.[1] Platelets are thought to occur during the formation of the B centers ($N_4V$), so they are closely associated with nitrogen defects.

This application note focuses on the $N_3VH$ defects, another type of nitrogen aggregate common in natural diamonds. A $N_3VH$ defect contains three N atoms substituting for C atoms arranged around a vacancy, along with a H atom bonded to the carbon next to the vacancy,[2] as shown in the ball-and-stick model in Figure 2. The characteristic IR features for the $N_3VH$ defects include the C-H stretching band at 3,107 $cm^{-1}$ and the C-H bending band at 1,405 $cm^{-1}$ (Figure 2).

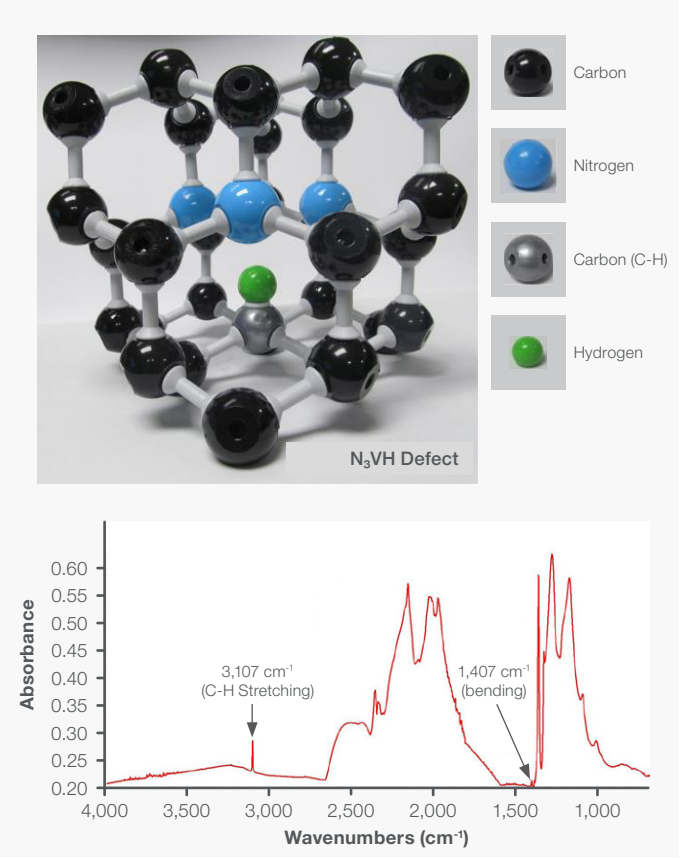


**Figure 2. The $N_3VH$ defect structure and an infrared spectrum showing the peaks associated with the stretching (3,107 $cm^{-1}$) and bending (1,407 $cm^{-1}$) of the C-H shown in the structure.**

FTIR mapping was used to observe the spatial distributions of the nitrogen-related defects. Visual images of the diamond sample and the area on the diamond selected for the analysis are shown in Figure 3a and 3b, respectively. The visual mosaic of the whole sample was collected using a 4X visual objective and the visual mosaic of the analysis region was collected using the 15X infrared objective. Infrared spectra were collected across the area of interest (25 µm steps). The peaks associated with different types of defects were used to create false-color images showing the intensity variation of the different defects across the area. The infrared images shown in Figure 3 are based on the intensities of the peaks indicated, where the red color indicates a higher intensity, the blue color a lower intensity, and the yellow and green colors intermediate intensities. Note that the color scale on each image is unique to that image and there is no direct relationship between the colors across different images. As shown in the FTIR images (Figure 3c-f), the platelets (1,362 $cm^{-1}$) and the B-center defects (1,330 $cm^{-1}$) are primarily located on the left side of the images. The most intense A-center defects (1,281 $cm^{-1}$) are located on the right side, but with some intensity in the general proximity of the platelets and the B-center defects. The $N_3VH$ defects (3,107 $cm^{-1}$) are mainly located in the center-bottom and right-middle. There is clearly a spatial correlation between the platelets (1,362 $cm^{-1}$) and the B-center defects (1,330 $cm^{-1}$), supporting the connection between the formation of B-centers and the platelets.

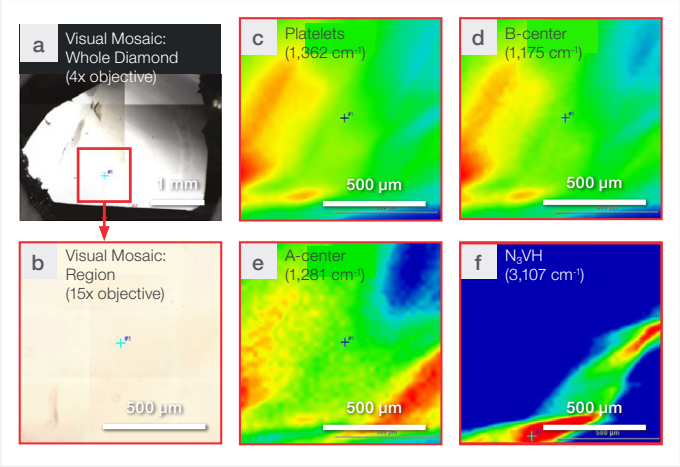


**Figure 3. Visual image of the whole diamond sample (a) and the region analyzed (b). (c) through (f) are infrared images showing the distributions of defects in the diamond sample generated from the peak intensities of the peaks indicated. Red (highest intensity) – Yellow – Green – Blue (lowest intensity). Specifically, the images show (c) 1,362 $cm^{-1}$ platelets; (d) 1,330 $cm^{-1}$ B-center; (e) 1,281 $cm^{-1}$ A center; and (f) 3,107 $cm^{-1}$ $N_3VH$ defect.**

The diamond sample was also analyzed by Raman imaging, and the resulting spectrum (Figure 4) gave both the expected diamond Raman peak as well as a PL peak at 613.17 nm (2.022 eV). This PL peak has been reported previously but the exact structure giving rise to the PL peak remains a topic for debate.[3] The same area used in the previous infrared measurements was imaged using the DXR3xi Raman Imaging Microscope. The visual images are shown in Figure 5 (5a and 5b). The peak intensity at 613 nm was used to create PL images (Figures 5c and 5d). Unlike the FTIR imaging experiments summarized in Figure 3, where each FTIR spectrum is a collective representation of the transmission measurements down through the whole sample thickness (z-axis), the confocal Raman microscope allows for data collection at a specific focal plane (one X-Y plane with a given Z value). The Raman image shown in Figure 5c is an image at one focal plane. The same area was imaged at different focal planes (different Z values) and the resulting series of 2-D images were then combined to generate a 3-D view of the sample (Figure 5d) showing a volume spatial distribution of the PL peak intensity.

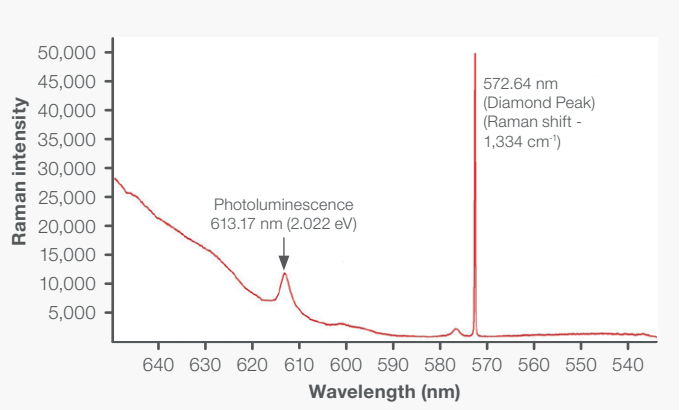


**Figure 4. Representative spectrum showing the Raman diamond peak (572.64 nm – 1,334 $cm^{-1}$) and the photoluminescent peak at 613.17 nm (2.022 eV).**

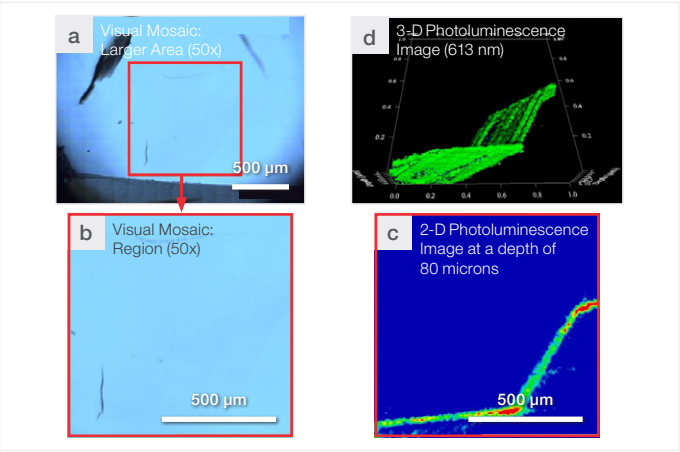


**Figure 5. (a) and (b) Visual mosaic images of the area analyzed. (c) 2-D image based on the intensity of the 613 nm photoluminescence peak at a depth of 80 microns into the sample (red is most intense and blue the lowest intensity). (d) 3-D view of the distribution of the photoluminescence peak intensity (613 nm).**

Of particular interest is the similarity in spatial distribution between the 3,105 $cm^{-1}$ peak in the infrared image and the 613 nm PL peak, as shown in Figure 6. Figure 6a is the infrared image based on the 3,107 $cm^{-1}$ peak. Note that this 2-D FTIR image obtained through transmission measurements is, in essence, a composite of all the confocal planes down through the whole sample thickness (Z-axis). For a better comparison, PL images at different focal planes (every 25 microns) were overlayed in Figure 6b to capture the overall lateral (X-Y) shifting of the peak intensity, as indicated in the selected 2-D PL images (Figures 6 c-f) as well as in the 3-D PL image (Figure 5d). It is worthwhile to mention that spatial resolution is 25 µm for FTIR imaging and 10 µm for Raman imaging, which also contributes to the observed difference in the width of the distributions between Figures 6a and 6b. There is perceivable resemblance in the 2-D contour of the $N_3VH$ defects in the FTIR image and the profile of the 613 nm peak in the PL image. While the current experiments do not suffice to conclude that the $N_3VH$ defects are the source of the 613 nm PL peak, the similarity in spatial distributions from two complementary spectroscopic techniques nonetheless suggests a strong relationship between them.

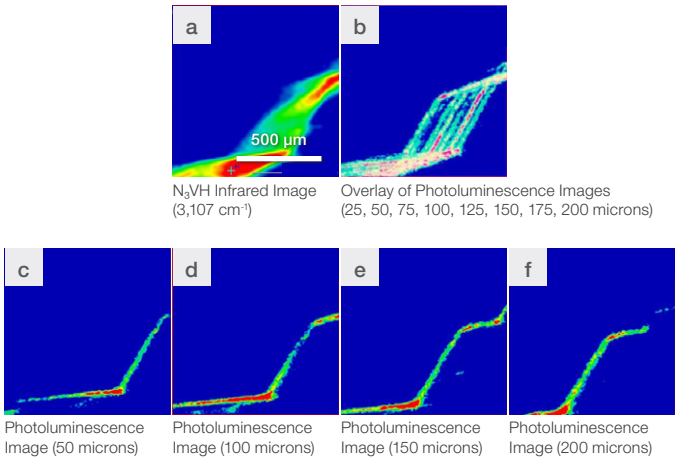


**Figure 6. Comparison (correlation) of the spatial distribution of the 3,107 $cm^{-1}$ peak of the $N_3VH$ defect (a) to an overlay of photoluminescence images from different focal planes (25, 50, 75, 100, 125, 150, 175, 200 µm). Images c-f are separate photoluminescence images at a few representative focal planes (50, 100, 150, 200 mm) , are included for comparison.**

## Conclusions:

In this application note, the infrared and PL imaging of a diamond sample is illustrated. Through FTIR imaging, the spatial distributions of different types of defects, including A-center, B-center, platelets, and $N_3VH$, were generated. A strong spatial correlation between the B-center defects and platelets was established. The spatial distributions of the PL peak at 613.17 nm observed during Raman imaging and the 3,107 $cm^{-1}$ peak observed in the FTIR map also showed a strong correlation. Since the 3,107 $cm^{-1}$ peak in FTIR is associated with the $N_3VH$ defects, the strong correlation suggests that the impurities/defects leading to the PL are closely related to the $N_3VH$ defects.

FTIR imaging, Raman imaging and PL spectroscopy are complementary techniques that together provide a comprehensive insight to diamond structure, defects, and impurities. FTIR excels in detecting impurities, characterizing defects, and type classification of diamonds. Raman is powerful in interrogating lattice vibrations, such as the changes induced by strain and stress, and studying inclusions. PL spectroscopy is particularly conducive to the investigation of luminescent properties and defect centers. Their combined use, such as the combination of the RaptIR+ Infrared Microscope and the DXR3xi Raman Imaging Microscope demonstrated in this application note, allows for cross-validation and holistic characterization, making these techniques essential tools in gemology and materials science.

### References


1. L. Speich, S.C. Kohn, R. Wirth, G.P. Bulanova, C.B. Smith, *The relationship between platelet size and the B' infrared peak of natural diamonds revisited*, Lithos 278-281, **2017**, 419-426.
2. Michael N. R. Ashfold, Jonathan P. Goss, Ben L. Green, Paul W. May, Mark E. Newton, Chloe V. Peaker, *Nitrogen in diamonds*, Chemical Reviews **2020** *120* (12), 5745-5794.
3. Jacob O. Woods, *An elusive impurity: studying hydrogen in natural diamonds*, Dissertation, University of Bristol, **2020**.


Learn more at **thermofisher.com/vibrational**